ACS Biomaterials SCIENCE & ENGINEERING
Article
Cite This: ACS Biomater. Sci. Eng. 2018, 4, 1324−1336

Incorporation of Nanoalumina Improves Mechanical Properties and Osteogenesis of Hydroxyapatite Bioceramics

Hossein Tavassoli,[†,‡,○,▲] Jafar Javadpour,[†] Mahdiar Taheri,[†,§] Morteza Mehrjou,[‡] Newsha Koushki,[∥] Farzin Arianpour,[†,▽] Mohammad Majidi,[‡] Jalal Izadi-Mobarakeh,[⊥] Babak Negahdari,[#] Peggy Chan,[○] Majid Ebrahimi Warkiani,[*,¶] and Shahin Bonakdar[*,‡]

[†]School of Metallurgy and Materials Engineering, Iran University of Science and Technology, P.O. Box 16846-13114, Tehran, Iran
[‡]National Cell Bank of Iran, [⊥]Physiology and Pharmacology Department, Pasteur Institute of Iran, P.O. Box 13169-43551, Tehran, Iran
[§]ANU College of Engineering & Computer Science, The Australian National University, Canberra, Australian Capital Territory 2601, Australia
[∥]Department of Bioengineering, McGill University, Montreal, Quebec, Canada H3A 0C3
[#]School of Advanced Technologies in Medicine, Department of Medical Biotechnology, Tehran University of Medical Sciences, Tehran, Iran
[○]Department of Biomedical Engineering, Swinburne University of Technology, Hawthorn, Victoria 3122, Australia
[▲]School of Mechanical and Manufacturing Engineering, University of New South Wales, Sydney, New South Wales 2052, Australia
[¶]School of Biomedical Engineering, University of Technology Sydney, Ultimo, New South Wales 2007 Australia
[▽]Research and Application Center, Kastamonu University, 37100 Kastamonu, Turkey

Supporting Information

ABSTRACT: A handful of work focused on improving the intrinsic low mechanical properties of hydroxyapatite (HA) by various reinforcing agents. However, the big challenge regarding improving mechanical properties is maintaining bioactivity. To address this issue, we report fabrication of apatite-based composites by incorporation of alumina nanoparticles (n-Al_2O_3). Although numerous studies have used micron or submicron alumina for reinforcing hydroxyapatite, only few reports are available about the use of n-Al_2O_3. In this study, spark plasma sintering (SPS) method was utilized to develop HA-nAl_2O_3 dense bodies. Compared to the conventional sintering, decomposition of HA and formation of calcium aluminates phases are restricted using SPS. Moreover, n-Al_2O_3 acts as a bioactive agent while its conventional form is an inert bioceramics. The addition of n-Al_2O_3 resulted in 40% improvement in hardness along with a 110% increase in fracture toughness, while attaining nearly full dense bodies. The in vitro characterization of nanocomposite demonstrated improved bone-specific cell function markers as evidenced by cell attachment and proliferation, alkaline phosphatase activity, calcium and collagen detection and nitric oxide production. Specifically, gene expression analysis demonstrated that introduction of n-Al_2O_3 in HA matrix resulted in accelerated osteogenic differentiation of osteoblast and mesenchymal stem cells, as expression of Runx-2 and OSP showed 2.5 and 19.6 fold increase after 2 weeks ($p < 0.05$). Moreover, protein adsorption analysis showed enhanced adsorption of plasma proteins to HA-nAl_2O_3 sample compared to HA. These findings suggest that HA-nAl_2O_3 could be a prospective candidate for orthopedic applications due to its improved mechanical and osteogenic properties.

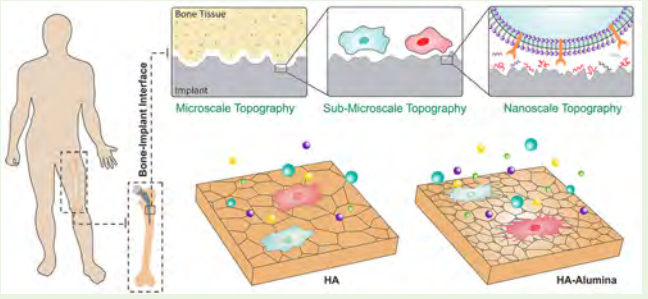

KEYWORDS: *hydroxyapatite, alumina, nanocomposite, osteoblast, adipose derived mesenchymal stem cells*

1. INTRODUCTION

A myriad of people around the world are suffering from orthopedic and bone diseases. For instance, just in the USA 332 000 total hip replacement (THR) and 719 000 total knee replacement (TKR) surgeries were performed in 2010. Estimates anticipated that by the year 2030, the number of THR and TKN revisions grow to 572 000 and 3.48 million procedures per annum, respectively.[1,2] Reconstruction of bone defects in load-bearing sites caused by a traffic accident, trauma, aging, infection or tumors has a socioeconomic burden for patients. Indeed, affected people endure great pain, besides the enormous medical cost is another major problem they are facing with during treatment.[3]

Accordingly, demands for finding new approaches and better ways to develop appropriate hard tissue replacement implants, having both abilities of binding to the surrounding tissue and

Received: October 9, 2017
Accepted: March 5, 2018
Published: March 5, 2018

DOI: 10.1021/acsbiomaterials.7b00754
ACS Biomater. Sci. Eng. 2018, 4, 1324−1336

match of mechanical properties, is a major challenge for materials communities and clinical researchers.[4]

Thanks to its chemical and structural similarity to mineral phase of natural bone and its outstanding bioactive properties, hydroxyapatite (HA) is generally recognized as a promising candidate for orthopeadic and dental implants. In spite of these favorable advantages (e.g., it has been considered as an osseointegrative and osteoconductive material), inherent poor mechanical properties of HA such as low fracture toughness (0.28−1.08 MPa $m^{1/2}$),[5] low wear resistance, and strength restrict its application for major load-bearing implants.[4,6]

Hence, a large number of researchers aimed to amend the mechanical reliability of HA by various methods.[7] In this context, one of the most prevalent techniques is the fabrication of apatite-based composites with second phase reinforcements such as yttria-stabilized zirconia (YSZ), alumina (Al_2O_3), zirconia (ZrO_2), titania (TiO_2), carbon nanotubes (CNTs),[5] strontium carbonate ($SrCO_3$),[8] Magnesium oxide (MgO)[9] and lanthanum oxide (La_2O_3).[10] Among different reinforcing agents, metal oxide ceramics such as ZrO_2, TiO_2, and Al_2O_3 has been widely used because of their high wear resistance, exceptional strength and fracture toughness as well as hardness. The striking benefit of using mentioned materials is their chemical inertness that does not compromise the biocompatibility of hydroxyapatite.[4,6]

Alumina is one of the most widely investigated reinforcement materials for HA bioceramics. It is mainly used as a substantial component in stress bearing areas such as total hip, shoulder and knee replacement.[11] In the past three decades, alumina has been investigated as a powerful contender for reinforcement of HA. To date, several researchers have studied various approaches to synthesize hydroxyapatite-alumina (HA-Al_2O_3) composites followed by characterization of microstructures and measurement of mechanical properties. In this regard, different mechanical properties (i.e., bending and compressive strength, fracture toughness and hardness) has been investigated. As summarized in Table S1, all the relevant studies about HA-Al_2O_3 composites are reviewed and different aspects of studies are compared.

An undesired problem associated with producing dense bodies of these composites is deleterious reactions between HA and reinforcing phase. On the other hand, during the sintering process decomposition of HA into α or β tricalcium phosphate (TCP) phase occurs which results in poor densification and reduced mechanical properties. Besides, formation of third phases (i.e., calcium aluminates phases) is another byproduct of these reactions. The formation of calcium aluminates phases has raised unresolved questions about their effect on biological and mechanical features of HA-Al_2O_3 composites.[12] In this context, several solutions have been developed to overcome the tendency of degradation of HA to tricalcium phosphate (such as the addition of CaF_2, MgF_2 or AlF_3 or calcination of starting powder[13,14]), whereas each of them has its drawbacks.

Therefore, an effective way to attain a full dense HA-Al_2O_3 compact without decomposition of HA is to take advantage of spark plasma sintering (SPS). SPS technology is a pressure-assisted sintering method in which high heating rates together with high voltage and pulsed direct current is applied resulted in a highly consolidated material, where can maintain the grain size similar to starting powder and suppress the diffusional time dependent reactions.

Although numerous studies in the literature used micron or submicron alumina for reinforcing hydroxyapatite composites, only a few publications are available concerning nano alumina (Table S1). Utilizing nano alumina has a significant effect on mechanical properties, therefore, in the modern era, it has attracted a large amount of attention. However, the most interestingly marvelous trait of nano alumina is its bioactive nature, which has rarely been investigated. Whereas conventional alumina is generally considered as a bioinert ceramic, Webster et al., have reported that osteoblast adhesion was significantly higher on nanophase alumina compared to its conventional form.[15] Furthermore, they demonstrated that nanophase alumina possessed enhanced functions of osteoblast cell (e.g., proliferation, alkaline phosphatase activity, and deposition of calcium-containing mineral) compared to conventional ones.[16] It has been proved that adsorption of specific proteins mediated enhanced cell functions regarding nanostructured alumina compacts.[17]

Considering the presented scenario, in this study nanocomposites comprising of HA and Al_2O_3 was synthesized and consolidated by SPS technique. Phase characterization, physical, and mechanical properties of samples were analyzed. In hard tissue engineering, the two important cell types are osteoblasts and mesenchymal stem cells (MSCs), as they play critical roles in bone homeostasis and remodeling. Therefore, in this study interaction of fabricated bioceramics with both bone forming cells and MSCs was studied via evaluation of cell proliferation, adhesion, various functions, and differentiation.

2. EXPERIMENTAL SECTION

2.1. Starting Materials and Mixing Conditions. Nanocrystalline alumina (Sigma-Aldrich, purity 99.99%) and HA (Sigma-Aldrich) powders with the average particle size of 50 and 60 nm were utilized as starting materials for samples preparation in this research. Figure S1A, B shows the scanning electron microscopy (SEM) images of as-received alumina and HA nanopowders. HA-Al_2O_3 nanocomposite powder mixtures containing 10, 20, 30 wt % of alumina as reinforcement were mixed and homogenized in a PTFE jar mill using ethanol (chemical grade, Merck Ag, Germany) for 24 h rotation time at the speed of 100 rpm, and the weight ratio of ball-to-powder was 10:1. The mixtures were gradually dried in a rotary evaporator under vacuum and passed through −60 mesh sieve to obtain a homogeneous powder. The composite samples were named as HA-10A, HA-20A, HA-30A, according to the percentage of alumina.

2.2. Sample Preparation via SPS Procedure. Bioceramic composite powders were consolidated using SPS (FCT HP D25/1) under vacuum (1×10^{-2} mbar). Powders were poured into a graphite die and a sheet of graphite was placed between the powders and die/punches to ease the specimen removal. Afterward, a fixed heating rate of 50 °C/min under a constant applied pressure of 50 MPa with a soaking time of 5 min was employed to produce disks with 20 mm diameter and approximately 5 mm thickness. An optical pyrometer was utilized to measure the temperature at about 4 mm from the sample. Soaking temperature of 1150 °C was selected for sintering pure HA and all three composites. Moreover, the sample containing 30 wt % of alumina was sintered at the higher temperature of 1250 °C to improve the density of the sample and obtain relative density higher than 95%. Nomenclatures of four sintered composites are tabulated in Table 1.

Moreover, during all sintering cycles, the height variations (displacement changes) of the samples (L_i) were directly monitored by means of a laser device. The instantaneous relative density (D_i) calculated by the eq 1:

$$D_i = (L_f/L_i)D_f \quad (1)$$

Where L_f and D_f are the final height and relative density of samples, respectively. The densification curves of the samples were plotted as relative density vs temperature (RD-T).

2.3. Characterization of Sintered Samples. X-ray diffraction (XRD) method was exploited to identify phases in the samples using Cu Kα radiation over the 2θ range of 20−60° at a scan rate of 0.01 (Philips PW1800, Netherlands). The specimens were ground and polished using

DOI: 10.1021/acsbiomaterials.7b00754
ACS Biomater. Sci. Eng. 2018, 4, 1324−1336

Table 1. Characteristics of Sintering Conditions for Pure HA and Composite Samples

notation	composition	sintering temperature (°C)	sintering time (min)	pressure (MPa)
HA	pure HA	1150	5	50
HA-10A	HA with 10% Al_2O_3	1150	5	50
HA-20A	HA with 20% Al_2O_3	1150	5	50
HA-30A	HA with 30% Al_2O_3	1150	5	50
HA-30A*	HA with 30% Al_2O_3	1250	5	50

diamond abrasive discs to remove the graphite contamination followed by fine polishing with 1 μm diamond solution. Then the specimens were thermally etched at 1050 °C for 15 min in air atmosphere. The microstructure of sintered sample was observed using a field-emission scanning electron microscope (FE-SEM, VEGA/TESCAN, Mira 3-XM). Energy-dispersive X-ray spectroscopy (EDX) and elemental mapping of the composite sample was studied using FEI Nova NanoSEM 450. Surface topography and roughness of polished and thermally etched samples were tested using atomic force microscopy (Bruker's dimension icon atomic force microscope (AFM)) in tapping mode. The scan rate was around 0.25 Hz, and scan size was 3 × 3 μm^2 with a resolution of 512 samples/line. Roughness values were evaluated from images taken at three random areas on each sample. The nano scope analysis software (version 1.7) was utilized to analyze the AFM results. To compare the wetting behavior of pure and composite sample, the hydrophilicity of samples was tested by water contact angle measurement using Kruss contact angle analyzer (DSA100) at three different locations of each sample. Density of the sintered samples was measured by Archimedes' water immersion principle. The theoretical densities of the composites were calculated based on the rule of the mixtures.

2.4. Evaluation of Mechanical Properties. Indentation test was performed using a diamond Vickers indenter under 0.5 and 5 kg loads for hardness and fracture toughness measurements, respectively, with a dwelling time of 20 s on the carefully polished surface of specimens. The hardness (H_V) was calculated from the diagonal length of the indentation using eq 2:[18]

$$H_V = 1.854\frac{P}{d^2} \tag{2}$$

Where P and d denote the applied load and the mean value of the diagonal length, respectively. Fracture toughness (K_{IC}, MPa $m^{1/2}$) was determined by measuring the crack length (indicated as C in Anstis' equation[19]) which measured immediately after indentation by means of an optical microscope.

$$K_{IC} = 0.016\left(\frac{E}{H_v}\right)^{0.5}\left(\frac{P}{C^{1.5}}\right) \tag{3}$$

Where E is the Young's modulus (GPa) calculated based on the rule of mixtures, H_V is the Vickers hardness (GPa), and P is the load (N). The average H_V and K_{IC} values were reported from at least ten valid measurements for each sample.

Since that final shaping of ceramic compacts is a striking phase for producing implants with complex geometry, quantitative evaluation of the machinability of the HA/Al_2O_3 composites was carried out by determination of brittleness index (BI) using eq 4.[19]

$$BI = \left(\frac{H}{K_{Ic}}\right) \tag{4}$$

Where H is the hardness and K_{Ic} is the fracture toughness. The average values of H and K_{Ic} were used for calculation.

2.5. Cell Culture Experiments. Prior to cell culture, HA and HA-20A ceramic discs were washed with 70% ethanol, sonicated in acetone, rinsed in distilled water and sterilized using an autoclave (121 °C, 20 min).

Osteoblast and adipose derived mesenchymal stem cells (ASCs) from white New Zealand Rabbit were freshly isolated based on Iran National Cell Bank established protocols under the ethical rules. For ASCs isolation, adipose tissue was dissected and incubated in collagenase solution (0.5%, Gibco) for 1 h under shaking to digest the tissue. Afterward, the cells were isolated by centrifugation and transferred to a 6 well tissue culture plate. For osteoblast isolation, a piece of bone was rinsed in culture medium and transferred into a 6 well tissue culture plate. During a period of 14 days, adhered cells were suspended and used for further analysis. The cells were cultured in Dulbecco's modified Eagles' medium (DMEM, Gibco, Scotland)/Ham's F12 (GIBCO, Scotland) supplemented with 10% Fetal Bovine Serum (FBS, Nanobioarray, Iran), 100 U/mL penicillin and 100 μg/mL streptomycin (Sigma, USA) at 37 °C in a humidified atmosphere consisting of 5% CO_2. Cells were detached by trypsin−EDTA solution and seeded on ceramic discs. A seeding density of 3×10^3 cells/cm^2 was applied for cell attachment and proliferation studies, while for osteogenic differentiation assays (i.e., alkaline phosphatase (ALP) activity, extracellular matrix (ECM) mineralization, collagen synthesis, nitric oxide (NO) production, and mRNA gene expression) cells were cultured at a higher density of 2×10^4 cells/cm^2 according to previously described protocol[20] unless otherwise noted.

2.6. Morphology, Attachment, and Growth of Seeded ASCs. Adhesion and spreading of ASCs seeded on the samples, was observed via SEM. After incubation for 4, 24, and 72 h, cells on the specimen surfaces were fixed with 2.5% glutaraldehyde (Sigma-Aldrich, Castle Hill, NSW, Australia) solution. Subsequently, fixed samples were washed with distilled water, dehydrated using a graded series of ethanol (30, 50, 70, 95, and 100%) for 10 min, dried using a solution of 50% ethanol and 50% hexamethyldisilazane (HMDS, Sigma-Aldrich, Castle Hill, NSW, Australia) for 5 min and exchanged with 100% HMDS for 10 min. Finally, cell seeded ceramic discs were sputter coated with gold (EMITECH K550) and observed by SEM (Hitachi S-3400).

2.7. Cell Proliferation Assay. The proliferation rate of ASCs cultured on ceramic discs was assessed by MTT (3-[4,5-dimethylthiazol-2-yl]-2,5-diphenyl tetrazolium bromide) assay. Briefly, 100 μL of culture medium containing 3×10^3 cells were seeded upon each sample in a 12-well culture plate. Plates were incubated in standard culture conditions (37 °C, 5% CO_2 and a humidified atmosphere) for 3 h, then 1.9 mL culture media was added to each well. After 7 and 14 days of culture, 500 μL of MTT solution (0.5 mg/mL) was added into each well, and the plate was kept in the incubator for 4 h. The generated purple crystals of formazan were dissolved in isopropanol (Sigma, USA) and the absorbance at an optical density (OD) of 540 nm was measured using a microplate reader (STAT FAX 2100, USA). Absorbance values were presented as percentages relative to control. Moreover, the cell proliferation in contact with biomaterials particulate debris was evaluated by colony formation assay. In brief, approximately 100 cells were cultured in a 6-well plate containing 100 μg/mL particles of each sample and growth medium. At day 14, the medium was discarded, cells were washed with PBS and fixed with glutaraldehyde (6.0% v/v). Finally, colonies were stained with crystal violet (0.5% w/v).

2.8. ALP Activity Assay. To determine the level of ALP activity of osteoblast and ASCs cultured on pure HA and composite samples, cells were cultured for 7 and 14 days under the same culture conditions as described in section 2.7. After detaching the cells from the sample surfaces according to Kaili Lin et al. study,[21] the relative ALP activity for each sample was assayed by measuring the amount of p-nitrophenol (pNP), the end product of hydrolyzed p-nitrophenyl-phosphate (pNPP) based on the instruction of manufacturer (Pars Azmun kit, Pars Azmun Co., Iran).[22]

2.9. Alizarin Red S (ARS) Staining and Quantitative Analysis. ECM mineralization of osteoblasts and ASCs was assessed by staining the calcium nodules formed after 7 and 14 days culture, as described previously.[23] In brief, at the predetermined time point the cells were fixed by paraformaldehyde (4%) for 10 min and stained with ARS solution (2%, pH 4.2) for 45 min at room temperature. The cells were rinsed twice with PBS to remove any further color and viewed by stereomicroscope (Nikon C-SD, Japan). For quantitative analysis of the mineralization process, 400 μL of 10 vol % acetic acid was added to each well, and the samples were incubated at 37 °C for 30 min. Cell layer was detached, transferred to a 1.5 mL microtube and heated at 85 °C for 10 min. They were placed into ice for 5 min and centrifuged at 20 000g

DOI: 10.1021/acsbiomaterials.7b00754
ACS Biomater. Sci. Eng. 2018, 4, 1324−1336

for 15 min at 4 °C. 80 μL from each sample was transferred to 96-well plate and 30 μL of 10 vol % ammonium hydroxide was added to neutralize the solution. The absorbance was measured in triplicate at 405 nm.

2.10. Collagen Production Assay: Sirius Red Staining. For collagen production measurement, Sirius red dye (Direct Red; Sigma, USA) was used to stain collagen. In this test, osteoblastic cells and ASCs were cultured in the same condition of previous tests. After 7 and 14 days of culture, staining was performed according to previously reported protocols.[24,25] The cell layers were extensively washed, then fixed and air-dried. Culture dishes stained with 0.1% Sirius red in saturated picric acid at room temperature for 1 h. The plates containing cells were washed with 0.01 N HCl three times to remove the unbounded dye. The stained cells were finally observed by a light microscope.

2.11. NO Production. Nitric oxide level was measured indirectly in cell culture supernatants using the Griess method.[26] A volume of 100 μL of supernatant from each sample was mixed with 100 μL of the mixture of Griess reagent A and B (1:1, v/v) (A: 1% sulfanilamide in 5% H_3PO_4, B: 0.1% naphtylenediamine in H_2O). After 30 min incubation, optical density was recorded at 540 nm using a spectrophotometer (STAT FAX 2100, USA) indicated the total level of nitrite in each sample and the concentration was calculated by means of $NaNO_2$ standard curve. Tissue Culture Polystyrene (TCPS) was considered as control similar to other tests. All experiments were performed in triplicate.

2.12. Quantitative Real Time Polymerase Chain Reaction (qRT-PCR). The osteogenic-associated gene expression for two distinct cell types (osteoblast and ASCs) were examined by quantitative real-time reverse transcriptase-polymerase chain reaction (qRT−PCR). Total cell RNA was isolated from the cells grown on each sample for 14 days using RNeasy Plus mini kit (Qiagen, 74104) and quantified by a spectrophotometer (Nanodrop, Germany). Subsequently, RNA was converted into complementary DNA (cDNA) via QuantiTect Reverse Transcription Kit (QIAGEN, Gaithersburg, MD), and finally, real-time PCR was performed in an ABI 7300 real-time PCR system (Applied Biosystems) with SYBR Green PCR master mix (Applied Biosystems). Gene expression was quantified using the ΔΔCt method. All experiments were performed in triplicate and the house keeping gene, Glyceraldehyde 3-phosphate dehydrogenase (GAPDH) was used as endogenous control. The primer sequence for runt-related transcription factor 2 (Runx-2), collagen type I (COL I) and osteopontin (OSP) are listed in Table S1.

2.13. Plasma Proteins Adsorption on Bioceramic Specimens. HA and HA-20A disks were incubated in Fetal bovine serum (FBS, Seromed, Germany) (with a concentration of 100 $\mu g.ml^{-1}$) at 37 °C in a humidified atmosphere to mimic the quasi-physiological conditions. After incubation for 4 and 24 h, samples were washed twice with deionized water to remove the loosely adherent proteins. To verify the protein adsorption to each sample, after rinsing with d-H_2O, we washed samples with 0.01, 0.1, and 1 M potassium chloride solutions based on previously published method.[27] Finally, an SDS-polyacrylamide gel electrophoresis (SDS-PAGE) procedure was employed to assess the KCl solution having adsorbed proteins, according to the Laemmli method.[28] Silver nitrate was used to stain the gels. To quantitatively study the amount of adsorbed proteins, we performed a Bradford assay.[29]

2.14. Statistical Analysis. All data were expressed as the average ± standard deviation (SD), and each experiment was repeated at least three times. Statistical comparison was examined by one-way analysis of variance (ANOVA) followed by a posthoc student's t test. Differences between groups were considered significant at $p < 0.05$.

3. RESULTS

3.1. Physical Properties and Phase Analysis. Figure 1A illustrates the relationship between relative density and sintering temperature during the heating part and dwelling at the maximum sintering temperature. A standard sintering sigmoidal curve with three main steps attributed to sintering of materials can be observed.[30] For example, in pure HA, the first step is less than 800 °C where there is almost no densification. It follows by an intense enhancement from 63 to 92% theoretical density when the temperature increases from 850 to 1100 °C. Finally, a slight improvement in relative density (up to 5%) happens in the last stage of sintering by raising the temperature from 1100 to 1150 °C. Furthermore, it can be observed that addition of alumina in composites influences the relative density of composite samples. The same trend in sintering of ceramic matrix composites has been reported in the literature where the second phase repressed diffusion mechanism during sintering.[22,31−33] When the alumina content increases, the density decreases. Because in this study, attaining a full dense structure with the best mechanical properties is the main challenge and the density pertained to HA-30A was much lower than other samples, the composite comprising 30% alumina was spark plasma sintered (SPSed) at an elevated temperature (i.e., 1250 °C) in order to have better densification. Relative densities of the sintered samples are compared in Figure 1C.

Figure S1A−C shows the high-resolution-SEM micrographs of the starting materials and the mixture of HA-30A after mechanical blending. One can observe well-dispersed alumina nanopowder without traces of agglomeration within HA powder. Uniform distribution of alumina phase throughout the composite is of great importance in terms of obtaining homogeneous mechanical properties and biocompatibility in the final implant. Therefore, results of elemental distribution of calcium, phosphorus, and aluminum studied by energy-dispersive X-ray mapping, indicates the uniform presence of alumina in HA matrix (see Figure S1D for more detail). The XRD pattern of SPSed pure HA and composites are shown in Figure 1B. XRD spectrum of as-received HA and alumina are also presented for comparison. For all the composite samples, characteristic peaks of HA are in good correspondence with the reference pattern (JCPDS no. 09−432). Furthermore, other diffraction peaks at 2θ values of 35.1, 37.7, 43.3, 52.5, and 57.5 matches strongly with those of Al_2O_3 standard diffraction file (JCPDS no. 10−173). In pure HA and all composite samples sintered at 1150 °C, no additional peaks were observed suggesting that no phase transition has been occurred. Increasing the sintering temperature to obtain better densification led to appearance of some new peaks in spectrum of HA-30A* sample. The emerged peaks were attributed to TCP phase. Dissociation of HA to TCP based on the following reaction is a prevalent reaction in conventional pressureless sintering that has been categorically proved above 1200 °C.

$$2Ca_5(PO_4)_3(OH) \rightarrow 3Ca_3(PO_4)_2 + CaO + H_2O$$

This reaction could be restricted in SPS because of its very short sintering time. Nevertheless, in some studies such as researches performed by Dubey et al.[34] and Feng and colleagues,[35] it has been shown that decomposition of HA to β-TCP occurs at temperatures higher than 1200 °C even during SPS. Hence, the presence of peaks of tricalcium phosphate in the later sample showed that sintering of the rather dense composite containing 30% of alumina was not achievable even during SPS method. Another critical finding of the present study is the absence of any calcium aluminate phases. A handful of work over the past decade focused on sintering of HA-Al_2O_3 composites using micron- and nanosized component. Conventional sintering in these studies leads to the formation of calcium aluminate phases (such as $CaO(Al_2O_3)_6$, $CaAl_4O_7$, $Ca_{12}Al_{14}O_{33}$, $Ca_3Al_2O_6$, $Ca_5Al_6O_{14}$, and $CaAl_2O_4$), a method in which diffusion plays a major role and alumina in this system leads to the formation of as mentioned calcium aluminate phases. Variation in sintering temperature ranging from 1000 to 1400 °C could not prevent such a phase transformation.[12] In this regard, SPS has been introduced as a reliable technique that enables the production of HA based composites without any reaction products and interestingly with

DOI: 10.1021/acsbiomaterials.7b00754
ACS Biomater. Sci. Eng. 2018, 4, 1324−1336

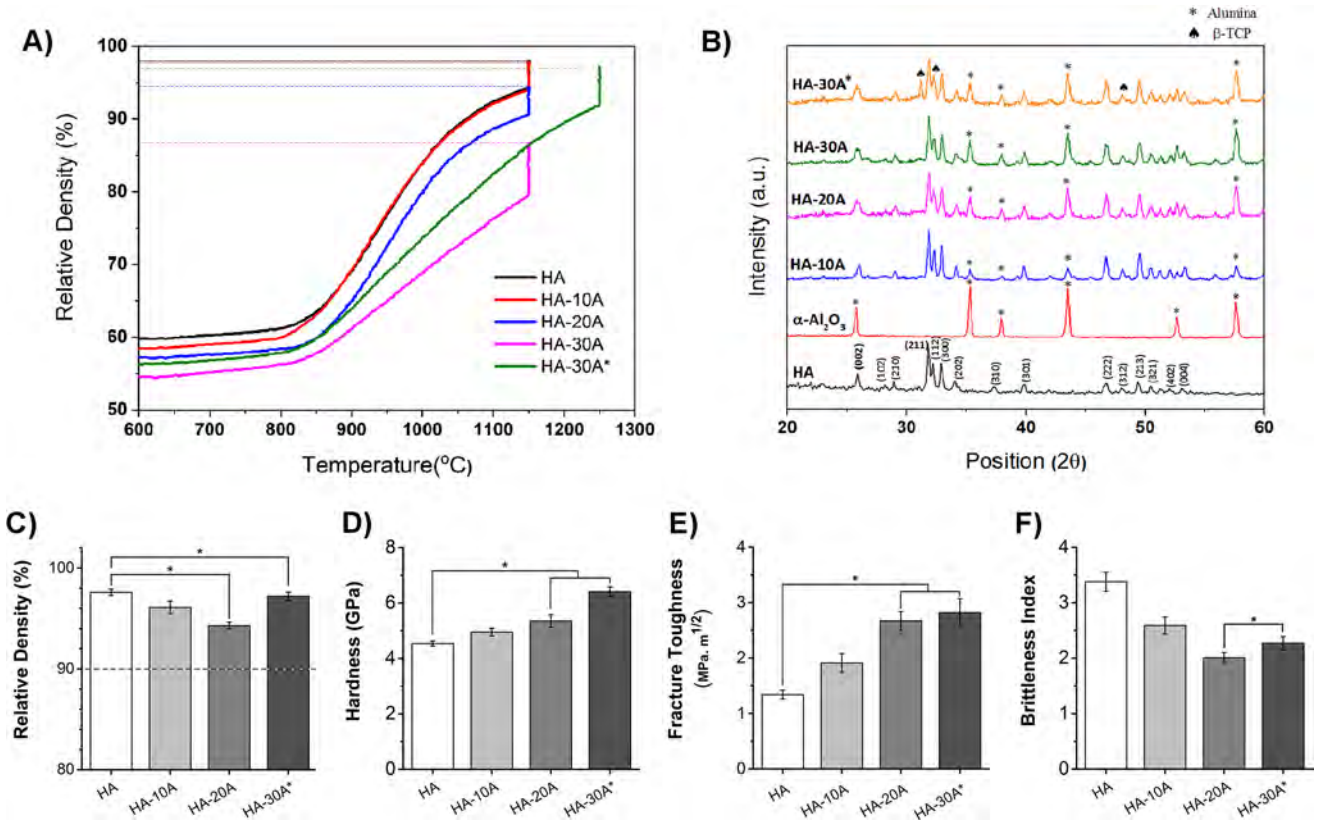

Figure 1. (A) Densification (relative density vs temperature) obtained in the pure HA and composites reinforced with different amounts of alumina nanopowder during spark plasma sintering. Because herein, attaining a fully dense structure with the best mechanical properties is the main challenge and the density of HA-30A was much lower than other samples, the composite comprising 30% alumina was spark plasma sintered at an elevated temperature (i.e., 1250 °C) to have better densification. (B) X-ray diffraction pattern of HA, alumina, and composite samples sintered via SPS. (C−F) Relative density and mechanical properties of HA/alumina composites. Because the difference between mechanical properties of HA-20A and HA-30A* is negligible, the brittleness index reached to the lowest amount for the HA-20A sample and the HA-30A* sample indicated decomposition in HA, the HA-20A sample was selected to study the biological properties.

much finer microstructure.[36] For example, HA-ZrO_2,[37] HA-mullite,[34] and recently HA containing only 20 wt % alumina in a functionally graded composite[38] have showed phase stability during SPS process.

3.2. Mechanical Characterization. Figure 1C−F presents the mechanical properties of pure HA and HA/Al_2O_3 composites including hardness, fracture toughness and brittleness index as well as their relative density. Because the density of HA-30A sample was less than 90% (as can be seen in Figure 1A), the mechanical properties of the mentioned sample were not evaluated. As can be seen in Figure 1C, the density of the samples decreases by increasing alumina nano powders content. Consequently, the specimen with the highest fraction of alumina nanopowder (30 wt %) was sintered at higher temperature to achieve similar relative density as its counterparts. The general trend of density is in logical agreement with previous studies[31] as the increase in the weight fraction of the second phase inhibited diffusion mechanism during sintering in the corresponding samples.

In regard to the hardness of the specimens, the hardness value of HA-30A* reaches to 6.41 GPa, which shows more than 40% improvement in comparison with the pure HA sample. Because alumina has higher intrinsic hardness and sintering process was successful in achieving near full dense samples without decomposition, the observed increment is in accordance with available results in the literature.[31,39]

The fracture toughness of the pure HA and its composites are also presented in Figure 1E. Because of the well-known mechanisms presented in the previous study of the authors about introducing second particle phase,[22,33,40] the fracture toughness of the samples presented in this paper augmented from 1.34 to 2.82 MPa $m^{1/2}$ by adding 30 wt % nano alumina into pure HA. This increment was about 110%, which is considerable comparing to previously published articles.[30,40]

It is noteworthy to mention that the difference between mechanical properties of HA-20A and HA-30A* is negligible, and the brittleness index reached to the lowest amount for the sample comprising of 20 wt % alumina. Considering Boccaccini's model for machinability of a candidate material for use as dental/bone implant, lower brittleness index (e.g., BI < 4.3 $\mu m^{-1/2}$) improves the machinability of ceramics.[19] Furthermore, as mentioned in previous part, the HA-30A* sample sintered in 1250 °C indicated the decomposition in HA. Hence, the HA-20A sample can be selected as a proper candidate to study the biological properties in the upcoming sections.

3.3. Cell Attachment and Proliferation. To evaluate cell adhesion and observe cell morphology on the specimens, ceramic discs cultured with ASCs were examined 4, 24, and 72 h after cell seeding by SEM. To observe the early attachment, cells were fixed after 4 h culture. It can be seen that at early stage attachment cells grew favorably on both samples and attached well with a rounded shape. Morphological examination of cells on the surface illustrated at a higher SEM magnification also confirms this trend (Figure S2A−D). Prolonging the culture time to 24 (Figure S2E, F and Figure 2A, B) and 72 h, cells started to spread

DOI: 10.1021/acsbiomaterials.7b00754
ACS Biomater. Sci. Eng. 2018, 4, 1324−1336

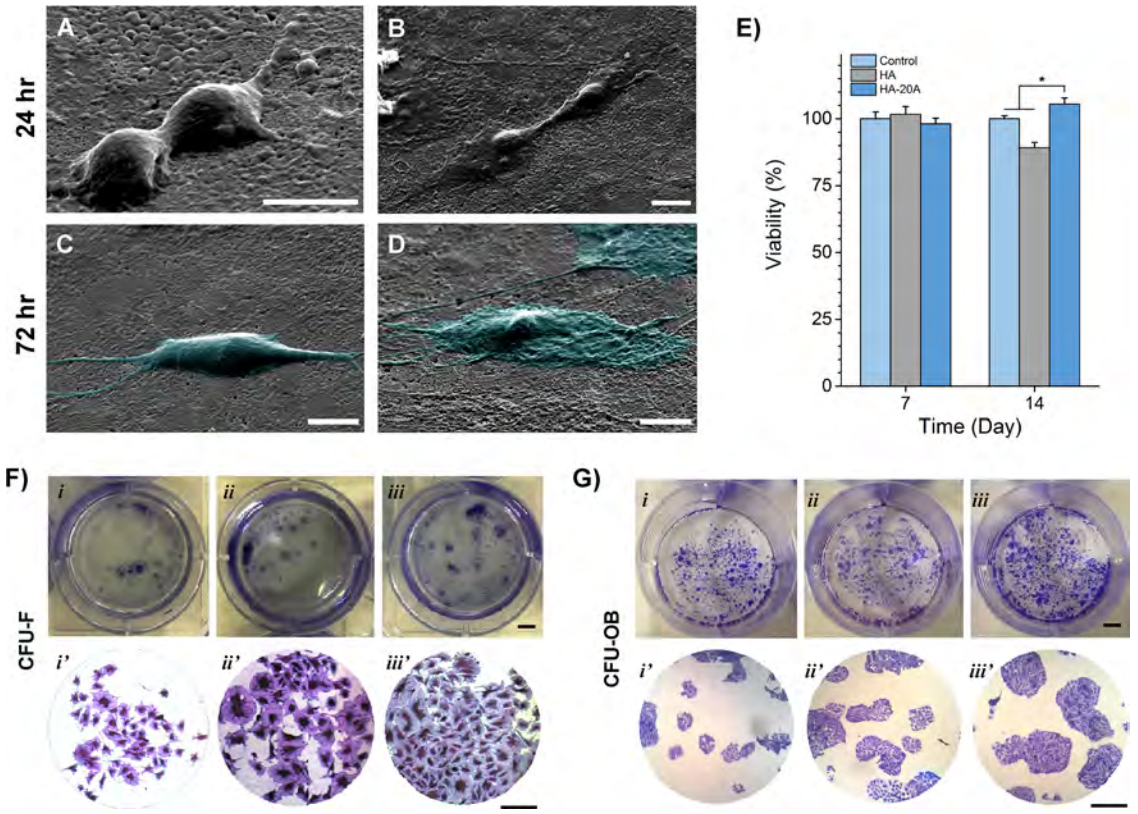

Figure 2. Proliferation, attachment, and growth of ASCs. (A) SEM images show cell attachment after 24 h on HA (A) and HA-20A (B), cells spread after 72 h on (C) HA and (D) HA-20A. To observe individual cell shapes, areas with a low cell density was selected. ASCs are pseudocolored turquoise to highlight spreading of cells. SEM images are taken by 60° tilting. Scale bars represent 10 μm in A-D images. (E) MTT assay for ASCs after seeding the cells for 7 and 14 days. HA-20A showed significantly higher cell viability ($P < 0.05$). Crystal violet staining of (F) ASCs and (G) osteoblast colonies after 2 weeks in growth media for (i) TCPS, (ii) HA, and (iii) HA-20A samples. Colony forming units for stem cells (CFU-F) and osteoblasts (CFU-OB) was much greater for the alumina-incorporated sample. Scale bars represent (i) 5 mm and (i′) 250 μm.

on the surfaces with growth of lamellipodia and filopodia. Morphology of attached single cells were also examined on pure and composite samples after 24 and 72 h. Figure 2 C, D displays the thoroughly flat cells after 72 h on each sample. Although HA surface is a favorable substrate, HA-20A sample provides a better environment, as can be seen in the higher density of cells (Figure S2E vs F), which are much flatter with more and longer filopodia, due to topographic effects. Both samples provide a proper surface to attach, anchor, and proliferate the cell on them. On the composite sample with nanosubmicron hybrid microstructure and topography, spreading and proliferation occurred faster. Quantitative evaluation of cell proliferation was measured using MTT assay. Results shown in Figure 2E demonstrate that cells grown on the HA-20A substrate and HA were able to proliferate well. However, after 7 days, the proliferation rate of cells cultured on HA was slightly higher compared to others, HA-20A specimen had significantly enhanced rate of proliferated cells after 14 days ($p < 0.05$). It should be mentioned that in Figure 2E, viability is displayed in percent (%), which means that for each time point the values for samples were normalized to the control values. The control values for 7 and 14 days were different, and the results showed that the values for 14 days were significantly higher than 7 days. Clonogenic assay results indicated that particulate of pure and composite sample showed no toxic effect on cells. The self-renewal capacity of examined cells in terms of ability to form colonies of osteoblasts (CFU-OB) and ASCs (CFU-F) visualized by crystal violet staining displayed that both osteoblast and stem cells in contact with ceramic particles retained the capacity to produce colonies after 2 weeks (Figure 2F, G). This ability was notably higher for ceramic samples containing alumina.

3.4. ALP Activity. ALP activity of osteoblast and ASCs cultured on the composite specimen for 7 and 14 days was investigated and compared with HA and TCPS as the control. Results showed in Figure 3A indicates an increase in ALP level after 7 days and a decrease for all samples at day 14 for osteoblast cells. It is well-known that alkaline phosphatase is considered as one of the essential markers of early osteogenesis. ALP activity was significantly higher for both HA-20A and HA as compared to control ($p < 0.05$). No significant difference was observed after 2 weeks of culture for control and HA samples. However, the composite sample had a stronger activity. This down regulation of ALP activity of osteoblast was observed in similar studies. Wang et al.,[41] investigated ALP activity of fluoridated-HA, observed this decrease in ALP activity, which shows cells stepped into the next differentiation stage. This enzymatic activity also had an increasing trend over time of assay for stem cells. Meanwhile, after 14 days, HA and composite samples had significantly higher values compared to control ($P < 0.05$), indicating the stem cells are at differentiation stages to osteoblastic lineage.

3.5. Mineralization Process and Quantitative Analysis. Figure 3B, C represents the results of ARS staining and quantitative analysis. Formation of mineralized nodules is apparent for ceramics specimens. Besides, after 14 days of culture, the presence of calcium deposits was higher for these samples. Figure 3C shows its corresponding quantitative analysis in which measured

DOI: 10.1021/acsbiomaterials.7b00754
ACS Biomater. Sci. Eng. 2018, 4, 1324−1336

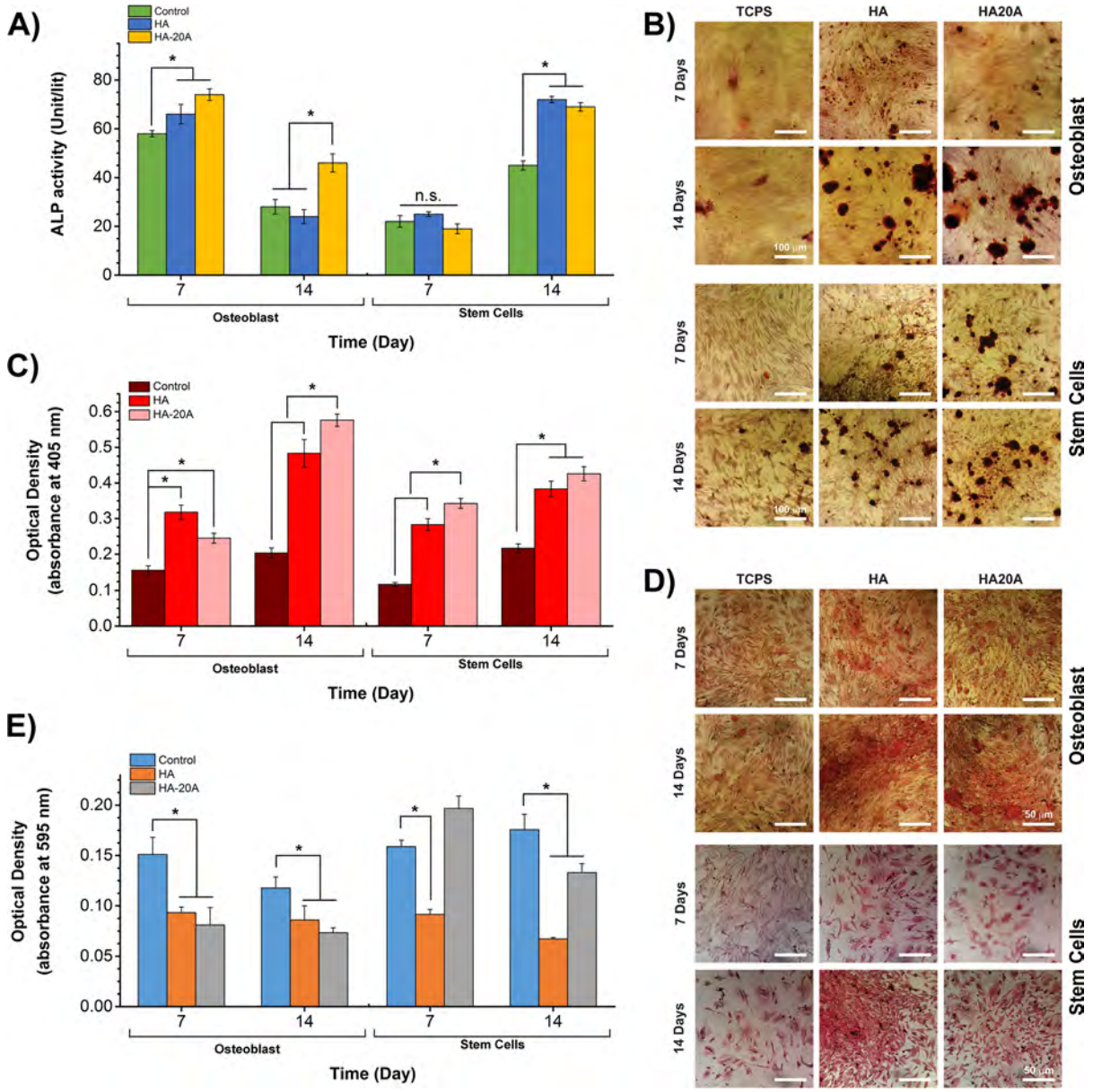

Figure 3. (A) ALP activity of osteoblast and ASCs after 7 and 14 days. HA-20A sample showed the highest amount of ALP activity for osteoblast and ASCs after 2 weeks culture. (B, C) Matrix mineralization and its quantitative analysis for Osteoblast and ASCs. Compared to control and HA, the composite sample showed more amount of ECM mineralization for both osteoblast and ACS after 2 weeks. (D) Sirius red staining of osteoblast and ASCs cultured for 7 and 14 days. Production of collagen after 14 days of culture was considerably higher for both ceramic samples compared to control. (E) Nitric oxide production of osteoblast and ASCs after 7 and 14 days. For osteoblast cells, NO production was significantly lower after 7 and 14 days of culture compared to HA and control. In case of ASCs, NO production for the composite sample was higher than HA, but was lowered compared to control after 2 weeks. Results are expressed as means ± SD, * denotes significant differences compared with the control ($p < 0.05$).

absorbance is significantly higher for cells cultured on HA and HA-20A compared with control sample ($p < 0.05$). Furthermore, ASCs grown on ceramic samples and specifically the composite one exhibited a greater amount of mineralization of ECM. Collectively, alumina-incorporated HA specimen revealed its positive role in calcium nodule formation at time of experiments compared to control samples for osteoblast and stem cells.

3.6. Sirius Red Staining. Staining of collagen content as a standard histological procedure[24] was performed in order to assess the collagen synthesis for osteoblast and ASCs. Figure 3D illustrates that some Sirius red stained spots apparently could be seen for composite specimen. Production of collagen after 14 days of osteoblast culture was considerably higher for both ceramic samples. ASCs cultured for 7 and 14 days also can secret a time dependent collagen, in which after 2 weeks, the highest amount of collagen production was determined for HA. Collagen staining also proved that HA-20A composite sample could motivate osteogenic differentiation of ASCs as can be seen in Figure 3D.

3.7. NO Production. Results of Griess assay demonstrates that osteoblasts had the lowest NO production in culture with HA-20A sample (Figure 3E). Nitric oxide has a mediatory role in cardiovascular hemostasis, immune function and bone resorption and formation.[42] In designing a material for orthopedic application, important criteria from a biological viewpoint is minimizing the immune response. For example, some applications like a coating for knee or hip implant requires high cell attachment and proliferation and low NP production.[26] It is well-demonstrated that low levels of NO could enhance the activity and

DOI: 10.1021/acsbiomaterials.7b00754
ACS Biomater. Sci. Eng. 2018, 4, 1324−1336

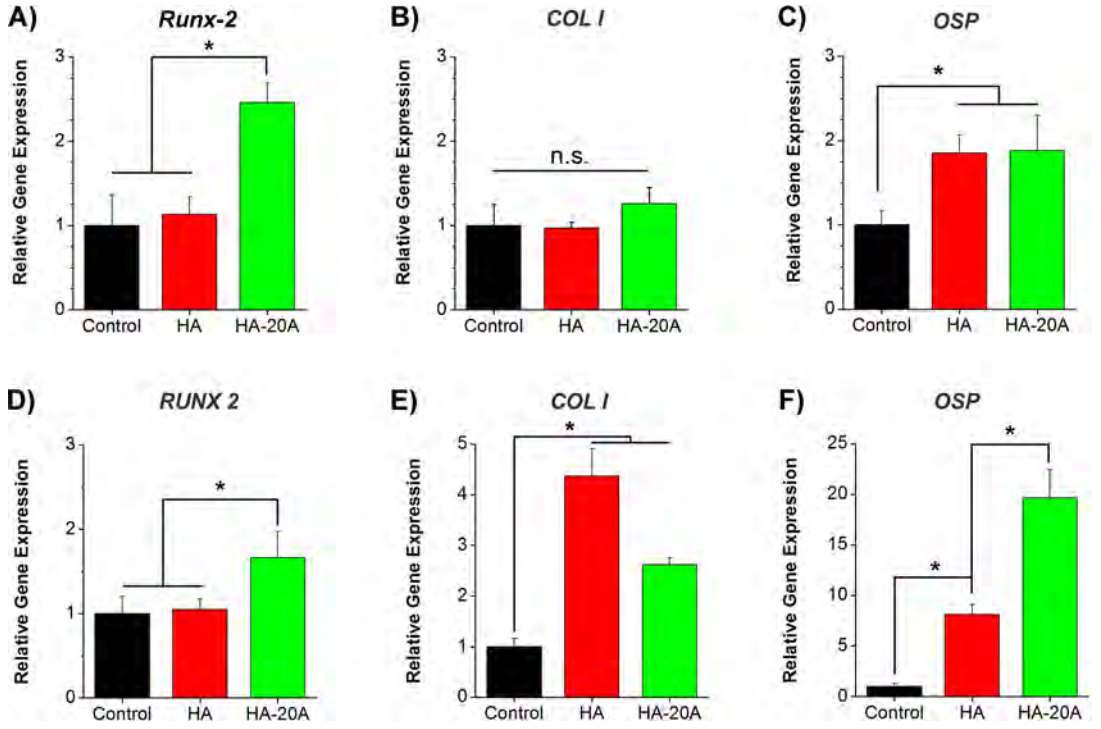

Figure 4. Gene expression results for osteogenic differentiation of (A−C) osteoblast and (D−F) ASCs. (A) Osteoblast cultured on HA-20A composite sample expressed significantly higher Runx2 compared to HA and control. (B) COL I was slightly upregulated in osteoblast cells cultured on HA-20A. (C) Expression of OSP for both ceramic samples was significantly higher in comparison to control. (D) Although no significant difference in Runx-2 expression level was observed for ASCs cultured on HA, up regulation took place for stem cells cultured on the composite specimen. (E) HA showed an enhanced level of OSP (up to 8.1 fold compared to control). An elevated level of COL I was also detected for HA and HA-20A. (F) ASCs cultured on the composite sample displayed greatest level of OSP expression compared to control (up to 19.6 fold). * denotes significant differences compared with the control ($p < 0.05$). ns represents no significant difference.

differentiation of bone cells.[42,43] Ralston et al. showed that cultured human osteoblast like cells produce NO in response to proinflammatory cytokines whereas this agent inhibits osteoblast proliferation.[44] Accordingly, the present data suggest that a considerably lower amount of NO produced in the SPSed composite sample will pose the effectiveness of manufactured sample. Cultured ASCs on HA showed significantly lower NO after 7 and 14 days. Although the highest nitric oxide was produced after 7 days culture for composite sample, it was reduced comparably with control at differentiation stage.

3.8. Gene Expression Analysis. The mRNA expression level of typical osteogenic markers, i.e., Runx-2, COL I, and OSP were analyzed by qRT-PCR. Osteoblast and ASCs were cultured for 14 days and results are shown in Figure 4. mRNA expression level of Runx-2 was markedly higher for composite sample and exhibited a 2.5 fold increase, whereas expression of OSP was enhanced for HA and HA-20A samples ($p < 0.05$). Compared to Control, COL I was slightly upregulated for osteoblast cells cultured on HA-20A. ASCs cultured on the composite sample displayed greatest level of OSP expression compared to control (up to 19.6 fold). Likewise, HA showed an enhanced level of OSP up to 8.1 fold compared to control. While no significant difference in Runx-2 expression level was observed for ASCs cultured on HA, up regulation took place for stem cells cultured on composite specimen. An elevated level of COL I was also detected for HA and HA-20A. RUNX2 is the most powerful determinant of osteogenic differentiation, a critical regulator during osteoblastic differentiation and mineralized tissue generation and it has a crucial role for induction of expression of other genes such as ALP, COL-I, etc.[45,46] The osteoblastic growth and differentiation is divided into distinct phases including self-renewal, lineage commitment, proliferation, ECM maturation, and matrix mineralization. At each stage, different markers are expressed that could be either upregulated or suppressed.[47] For example, ALP and Col-I could be in down regulation phase as they inherently go up and down at certain times of differentiation.[48]

According to a study[49] that compared gene expression of primary mouse and human bone marrow mesenchymal stem cell on different surface features ranging from sub nano, nano, submicron to micron, expression levels of Runx-2, COL I, and OSP were significantly higher on nanosubmicron titanium surface features. Evidences from this study explained that only nanosubmicron hybrid surface features activated α_1, α_2, α_5, and α_v integrins, which finally leads to stronger gene pathways for Runx-2, COL I, and OSP. Although other topographical features activated only α_2 and α_5 integrins.[49] Besides, in a recent study, Yang et al. reported an increasing expression level of OPN for human bone marrow mesenchymal stem cell cultured on a near square arrangement of nano pits (NSQ50) over a 4 weeks timecourse.[50]

3.9. Protein Adsorption on Substrates. Plasma protein adsorption behavior on the HA and HA-20A surfaces was studied via 1D SDS-PAGE analysis. As can be seen in the Figure 5, the bands' intensity in the protein profile of the HA-20A sample was stronger after 2 h of adsorption. This behavior was also recorded for extended time of 24 h. Figure 5C, D shows the amount of adsorbed protein onto the surface of samples investigated by Bradford assay. The adsorption amount of proteins in each stage of washing demonstrated in this graph, states that washing with 0.1 M KCl solution was more effective in isolating adsorbed protein in comparison with other solutions. Moreover, amount

DOI: 10.1021/acsbiomaterials.7b00754
ACS Biomater. Sci. Eng. 2018, 4, 1324−1336

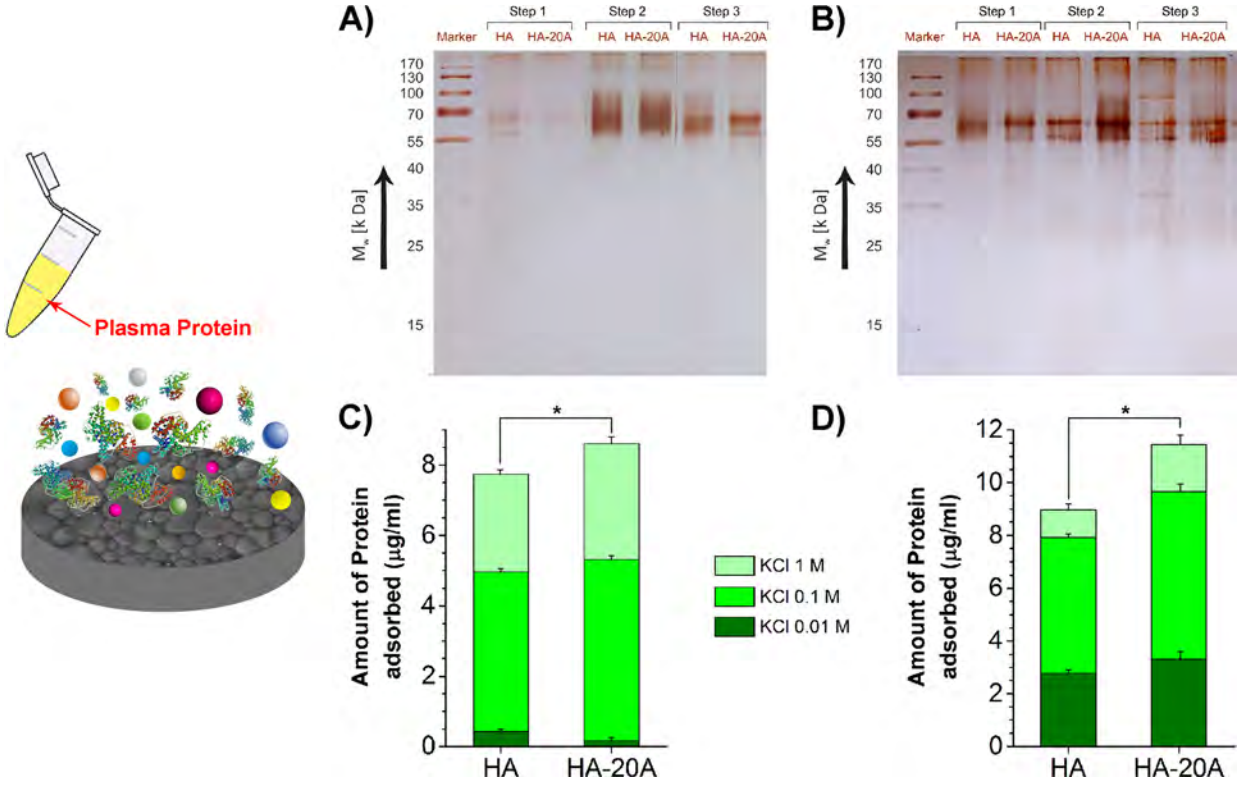

Figure 5. Plasma protein adsorption behavior on HA and HA-20A sample. A and C represent SDS-PAGE analysis and Bradford assay results for protein adsorption after 4 h. B and D correspond the results for protein adsorption after 24 h.

of proteins adsorbed on composite sample was significantly higher (8.6 and 11.5 μg/mL for 2 and 24 h of exposing time) compared to HA substrate. This finding was consistent with the results of protein electrophoresis experiment. It was worth mentioning that the considerable amounts of high molecular weight proteins (i.e., molecular weight of 66 kDa, such as albumin) are seen in electrophoresis pattern.

3.10. Surface Properties of Ceramic Samples.

Figure 6A–C displays the SEM as well as AFM images of the polished and subsequently thermal-etched surface of HA and HA-20A samples. The average grain sizes of the HA and HA-20A samples were calculated to be 580 and 310 nm, respectively. It can be comprehended that alumina nanoparticles are located in the grain boundaries and hindered the grain growth of HA particles during the sintering process. Ji et al.[51] reported the same trend by adding alumina micro particles into HA matrix sintered conventionally at 1200 °C. In this study, achieving such fine matrix in HA composite is related to the rapid sintering method and homogeneously dispersion of nano alumina in the matrix. High-resolution microscopy and AFM images revealed the presence of micron/submicron features on HA surface and submicron/nano features on the composite surface. Surface roughness values of ceramic surfaces (i.e., Ra and Rq) are compared in Figure 6D, E. Average Ra values for HA and HA-20A are 46.3 and 34.5 nm and RMS are 56.1 and 43.5 nm, respectively. This decrease in roughness values is in agreement with the previous studies, whereas Khang et al.[49] reported decrease in surface roughness for titanium surfaces with subnano, nano and submicron surface features. Due to decreased average surface roughness, protein adsorption was enhanced for composite sample. The static contact angle (CA) measurement showed that both surfaces have hydrophilic behavior. HA as a bioactive material has a hydrophilic surface with a mean value of 59.5 ± 2.2. The difference of CA for pure and composite sample is not significant, as mean wetting angle for HA-20A was 56.5 ± 4.3 (Figure 6 (F-G)). The relationship between wettability and surface roughness was studied in detail by Wenzel.[52] Moreover, Cassie–Baxter equation[53] states that for chemically heterogeneous surfaces with two different chemistries, surface wettability is altered by adding second surface roughness and chemistry.[54,55] Altogether, altered roughness along with surface wettability of HA-20A enhanced the protein adsorption of composite sample.

4. DISCUSSION

In response to increasing demand to find proper biomaterials for patients suffering the orthopedic and dental problems, many studies have been performed in the last decades. Clinical success of an implant in long-term periods is related to early events of osseointegration of implant. In this regard, surface modification of implants has attracted much attention in terms of modification of surface roughness, chemistry and wettability. Research studies analyzing various surface roughness from subnano and nano to submicron and micron size[49,56] showed that the surfaces having hybrid features of nanosubmicron–micron scale are necessary for improved protein adsorption, anchorage-dependent osteogenic cells adhesion, growth and subsequently enhanced cellular function and stimulated osseointegration in vivo. In most of the studies, titanium nano/micro particles are coated on a transparent coverslip for ease of simulation of osteoblast or stem cell interaction with biomaterials. In this study, we aimed to develop a hydroxyapatite based ceramic with improved mechanical and bioactivity properties. Physical and mechanical characteristics of HA containing 20 wt % alumina was improved compared with HA. Chemical and phase analysis of bulk and surface of HA-20A (as revealed by EDX and XRD), along with wettability and roughness examination (as revealed by water contact angle

DOI: 10.1021/acsbiomaterials.7b00754
ACS Biomater. Sci. Eng. 2018, 4, 1324–1336

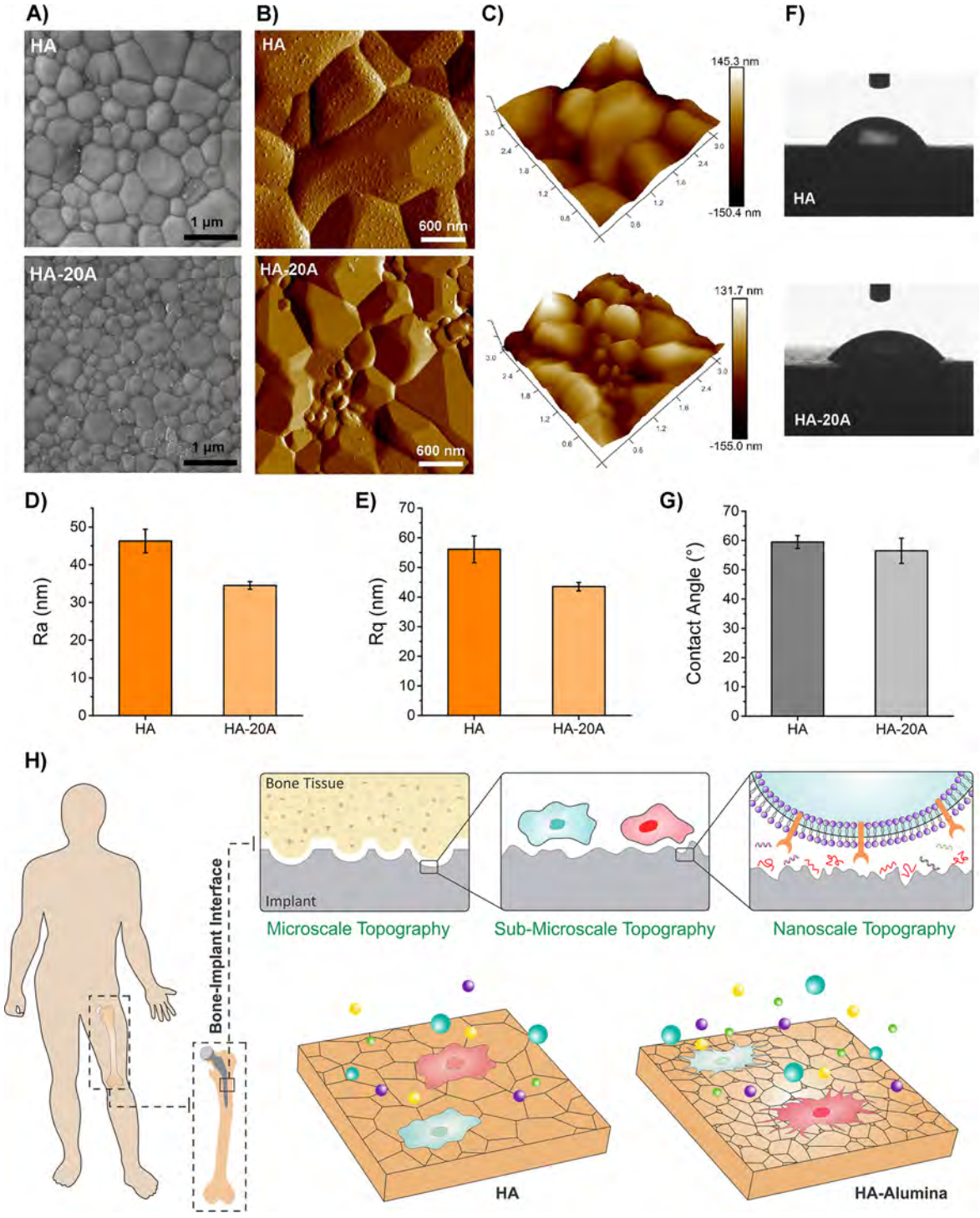

Figure 6. Surface analysis of bioceramics. (A) SEM images of the polished and subsequently thermal-etched pure HA and HA-20A composite. Scale bar is 1 μm. (B–E) Representative AFM amplitude, topographical images and roughness values for HA and HA-20A after polishing and subsequently thermal-etching, (B) 2D Amplitude representative images. (C) 3D topographical representative images. The AFM image was processed by first order flattening using NanoScope analysis software. (D, E) Corresponding R_a and R_q (RMS) surface roughness of HA and HA-20A after polishing and thermal etching. (F, G) Water contact angles of HA and HA-20A indicating the surface wettability of the substrates. (F) Optical images of water contact angles and (G) corresponding values on HA and HA-20A composite. (H) Schematic representation of bone/implant interaction and role of different topographies required for a successful osseointegration. The HA-Al_2O_3 composite sample has the combinatorial micron-submicron-nano features on the surface, as well as the presence of alumina nanoparticles as the bioactive agent results in higher initial protein adsorption, cell attachment, and differentiation.

measurements and AFM), showed that the presence of alumina nano grains at the grain boundaries of micron and submicron sized HA grains favors initial protein adsorption and subsequent cell adhesion and growth. Previous studies by Webster group[16,17] proved that nanophase alumina is bioactive while its conventional micron size is considered bio inert. Hence, not only alumina nano grains that dispersed in the microstructure of developed composite act as a bioactive site for protein adsorption, subsequent bone cellular

DOI: 10.1021/acsbiomaterials.7b00754
ACS Biomater. Sci. Eng. 2018, 4, 1324–1336

functions was also improved. There is a direct relation between serum proteins adsorption capacity of a surface and successive cell adhesion and growth,[57] so plasma proteins directly mediate cellular adhesion and spreading. It was found that HA-nAl_2O_3 adsorbed up to 8.6 and 11.5 μg/mL of proteins after 4 and 24 h, compared to 7.6 and 8.9 μg/mL on HA surface. Since the size of proteins and cell membrane receptors (such as focal adhesion sites) are in nano magnitude, heterogeneous features size of HA-20A composite is comparable to resorption pits and cell dimensions (Figure 6H). HA-nAl_2O_3 composite also showed great results regarding mesenchymal stem cell fate. Stem cells located in a bone niche (e.g., mesenchymal, hematopoietic, etc.) will contribute to bone regeneration and healing of surrounding bone after clinical insertion of an implant. ASCs exhibited faster cell attachment and spreading, improved proliferation and enhanced cell functions and differentiation. It should be also noted that in all experiments, culture media was normal growth media without use of osteogenic stimulating factors like dexamethasone, BMP-2 or other growth factors. This indicates that the bioactive HA-Al_2O_3 composite can be used in various orthopedic applications like bone/dental fillers and implants and tissue engineered scaffolds. This material as monolith can be used as middle ear implant that currently is made of apatite-wollastonite (A-W) glass ceramics as artificial middle ear bone implant.[58−60] HA alone does not have the proper strength to be used but the HA-20A which has improved mechanical properties with enhanced bioactivity could be used as load bearing implant for small defects. It is worthwhile to mention that the current challenge in the fabrication of tissue engineered scaffold is the weakness of the scaffolds when they have a highly porous structure. The higher the porosity, the faster the degradation rate is. Because this material has a high mechanical strength, it can be made at a higher porosity that automatically compensates its chemically inherent low degradability.

5. CONCLUSIONS

In this study, nano alumina (nAl_2O_3) was added to nano hydroxyapatite (HA) structure to improve the physical-mechanical properties as well as the biological activity. The incorporation of nAl_2O_3 followed by spark plasma sintering resulted in a microstructure of combined submicron/micron-sized HA and nano-sized Al_2O_3 grains. HA-nAl_2O_3 without any calcium aluminate phases has the improved mechanical behavior as evidenced by density, hardness, toughness and machinability measurements, as well as enhanced biological activity. Nearly full dense composite samples containing nAl_2O_3 exhibited superior hardness values up to 6.41 GPa (more than 40% improvement in comparison with the pure HA) along with elevated fracture toughness values up to 2.82 MPa.$m^{1/2}$ (about 110% increase compared to pure HA sample). Primary osteoblasts and mesenchymal stem cells cultured on HA-nAl_2O_3 showed significantly higher attachment and proliferation, bone cell functions and expression of osteogenic differentiation markers compared to HA. Overall, the results suggest that HA-nAl_2O_3 has the potential application to be used as filler, implant, and scaffold material for middle ear, bone, and gingival defects because of its excellent mechanical properties coupled with its bioactivity.

■ ASSOCIATED CONTENT

Supporting Information

The Supporting Information is available free of charge on the ACS Publications website at DOI: 10.1021/acsbiomaterials.7b00754.

Table S1, a review of all the relevant publication about HA-Al_2O_3 composites from 1992 up to now, presents various approaches for synthesis, sintering, phase characterization, and mechanical and biological properties evaluation in each study, to highlight the significance of the present work compared to previous studies; Table S2, primers for real-time PCR; Figure S1, SEM images and EDAX of the starting powders and composite powder; Figure S2, SEM images of cell attachment after 4 and 72 h in different magnifications (PDF)

■ AUTHOR INFORMATION

Corresponding Authors

*E-mail: majid.warkiani@uts.edu.au (M.E.W.).
*E-mail: sh_bonakdar@pasteur.ac.ir (S.B.).

ORCID

Hossein Tavassoli: 0000-0002-4984-2482

Author Contributions

H.T., S.B., J.J., B.N., and J.I.-M. designed the research. H.T., M.T., and F.A. performed materials preparation and mechanical testing. H.T., N.K., M.Me., and M.Ma. performed the biological analysis. H.T. performed the microscopy characterizations parts. H.T., B.N., P.C., and M.E.W. performed data analysis. H.T., S.B., and M.T. wrote the manuscript.

Notes

The authors declare no competing financial interest.

■ ACKNOWLEDGMENTS

Research reported here was supported by the Iran Pasteur Institute with research project No. 861. We thank Dr Iman Roohani (School of Chemistry, UNSW) for insightful comments and discussions on the manuscript. We thank Dr. Shahram Azari and Mozhgan K. Moghadam (Iran Pasteur Institute) for technical support in protein analysis. H.T. is particularly grateful to Dr. Simon Hager and Mr. Yin Yao (Mark Wainwright Analytical Centre, Electron Microscope Unit, UNSW), Dr. Pramod Koshy (School of Materials Science and Engineering, UNSW), as well as Prof. Alexey Kondyurin (School of Physics, University of Sydney) for kindly doing contact angle measurements.

■ REFERENCES

(1) Kurtz, S.; Ong, K.; Lau, E.; Mowat, F.; Halpern, M. Projections of primary and revision hip and knee arthroplasty in the United States from 2005 to 2030. *J. Bone Joint Surg Am.* **2007**, *89* (4), 780−785.

(2) Vahabzadeh, S.; Roy, M.; Bandyopadhyay, A.; Bose, S. Phase stability and biological property evaluation of plasma sprayed hydroxyapatite coatings for orthopedic and dental applications. *Acta Biomater.* **2015**, *17*, 47−55.

(3) García-Gareta, E.; Coathup, M. J.; Blunn, G. W. Osteoinduction of bone grafting materials for bone repair and regeneration. *Bone* **2015**, *81*, 112−121.

(4) Suchanek, W.; Yoshimura, M. Processing and properties of hydroxyapatite-based biomaterials for use as hard tissue replacement implants. *J. Mater. Res.* **1998**, *13* (01), 94−117.

(5) Kalmodia, S.; Goenka, S.; Laha, T.; Lahiri, D.; Basu, B.; Balani, K. Microstructure, mechanical properties, and in vitro biocompatibility of spark plasma sintered hydroxyapatite−aluminum oxide−carbon nanotube composite. *Mater. Sci. Eng., C* **2010**, *30* (8), 1162−1169.

(6) Ahn, E. S.; Gleason, N. J.; Nakahira, A.; Ying, J. Y. Nanostructure processing of hydroxyapatite-based bioceramics. *Nano Lett.* **2001**, *1* (3), 149−153.

(7) Basu, B.; Katti, D. S.; Kumar, A. *Advanced Biomaterials: Fundamentals, Processing, And Applications*; John Wiley & Sons: New York, 2010. 10.1002/9780470891315

DOI: 10.1021/acsbiomaterials.7b00754
ACS Biomater. Sci. Eng. 2018, 4, 1324−1336

(8) Gautam, C.; Tamuk, M.; Manpoong, C.; Gautam, S.; Kumar, S.; Singh, A. K.; Mishra, V. Microwave synthesis of hydroxyapatite bioceramic and tribological studies of its composites with SrCO3 and ZrO2. *J. Mater. Sci.* **2016**, *51* (10), 4973−4983.
(9) Gautam, C.; Kumar, S.; Biradar, S.; Jose, S.; Mishra, V. K. Synthesis and enhanced mechanical properties of MgO substituted hydroxyapatite: a bone substitute material. *RSC Adv.* **2016**, *6* (72), 67565−67574.
(10) Gautam, C.; Kumar, S.; Mishra, V. K.; Biradar, S. Synthesis, structural and 3-D architecture of lanthanum oxide added hydroxyapatite composites for bone implant applications: Enhanced microstructural and mechanical properties. *Ceram. Int.* **2017**, *43* (16), 14114−14121.
(11) Piconi, C.; Condò, S.; Kosmăc, T., Alumina and zirconia based ceramics for load-bearing applications. In *Advanced Ceramics for Dentistry*; Elsevier: Amsterdam, 2013; Vol. *219*, p 219. 10.1016/B978-0-12-394619-5.00011-0
(12) Viswanath, B.; Ravishankar, N. Interfacial reactions in hydroxyapatite/alumina nanocomposites. *Scr. Mater.* **2006**, *55* (10), 863−866.
(13) Evis, Z.; Doremus, R. H. Effect of AlF3, CaF2 and MgF2 on hot-pressed hydroxyapatite−nanophase alpha-alumina composites. *Mater. Res. Bull.* **2008**, *43* (10), 2643−2651.
(14) Kim, S.; Kong, Y.-M.; Lee, I.-S.; Kim, H.-E. Effect of calcinations of starting powder on mechanical properties of hydroxyapatite−alumina bioceramic composite. *J. Mater. Sci.: Mater. Med.* **2002**, *13* (3), 307−310.
(15) Webster, T. J.; Siegel, R. W.; Bizios, R. Osteoblast adhesion on nanophase ceramics. *Biomaterials* **1999**, *20* (13), 1221−1227.
(16) Webster, T. J.; Ergun, C.; Doremus, R. H.; Siegel, R. W.; Bizios, R. Enhanced functions of osteoblasts on nanophase ceramics. *Biomaterials* **2000**, *21* (17), 1803−1810.
(17) Webster, T. J.; Ergun, C.; Doremus, R. H.; Siegel, R. W.; Bizios, R. Specific proteins mediate enhanced osteoblast adhesion on nanophase ceramics. *J. Biomed. Mater. Res.* **2000**, *51* (3), 475−483.
(18) Wachtman, J. B.; Cannon, W. R.; Matthewson, M. J. *Mechanical Properties of Ceramics*; John Wiley & Sons: New York, 2009. 10.1007/978-3-319-04492-7
(19) Boccaccini, A. Machinability and brittleness of glass-ceramics. *J. Mater. Process. Technol.* **1997**, *65* (1), 302−304.
(20) Liu, Q.; Cen, L.; Yin, S.; Chen, L.; Liu, G.; Chang, J.; Cui, L. A comparative study of proliferation and osteogenic differentiation of adipose-derived stem cells on akermanite and β-TCP ceramics. *Biomaterials* **2008**, *29* (36), 4792−4799.
(21) Lin, K.; Xia, L.; Gan, J.; Zhang, Z.; Chen, H.; Jiang, X.; Chang, J. Tailoring the nanostructured surfaces of hydroxyapatite bioceramics to promote protein adsorption, osteoblast growth, and osteogenic differentiation. *ACS Appl. Mater. Interfaces* **2013**, *5* (16), 8008−8017.
(22) Mohamed, E.; Taheri, M.; Mehrjoo, M.; Mazaheri, M.; Zahedi, A.; Shokrgozar, M.; Golestani-Fard, F. In vitro biocompatibility and ageing of 3Y-TZP/CNTs composites. *Ceram. Int.* **2015**, *41* (10), 12773−12781.
(23) Koushki, N.; Katbab, A. A.; Tavassoli, H.; Jahanbakhsh, A.; Majidi, M.; Bonakdar, S. A new injectable biphasic hydrogel based on partially hydrolyzed polyacrylamide and nanohydroxyapatite as scaffold for osteochondral regeneration. *RSC Adv.* **2015**, *5* (12), 9089−9096.
(24) Tullberg-Reinert, H.; Jundt, G. In situ measurement of collagen synthesis by human bone cells with a Sirius Red-based colorimetric microassay: effects of transforming growth factor β2 and ascorbic acid 2-phosphate. *Histochem. Cell Biol.* **1999**, *112* (4), 271−276.
(25) Castrén, E.; Sillat, T.; Oja, S.; Noro, A.; Laitinen, A.; Konttinen, Y. T.; Lehenkari, P.; Hukkanen, M.; Korhonen, M. Osteogenic differentiation of mesenchymal stromal cells in two-dimensional and three-dimensional cultures without animal serum. *Stem Cell Res. Ther.* **2015**, *6* (1), 167.
(26) Liu, H.; Yazici, H.; Ergun, C.; Webster, T. J.; Bermek, H. An in vitro evaluation of the Ca/P ratio for the cytocompatibility of nano-to-micron particulate calcium phosphates for bone regeneration. *Acta Biomater.* **2008**, *4* (5), 1472−1479.
(27) Montazeri, L.; Javadpour, J.; Shokrgozar, M.; Bonakdar, S.; Khayyat Moghaddam, M.; Asgary, V. The interaction of plasma proteins with nano-size fluoride-substituted apatite powders. *Ceram. Int.* **2013**, *39* (6), 6145−6152.
(28) Laemmli, U. K. Cleavage of structural proteins during the assembly of the head of bacteriophage T4. *Nature* **1970**, *227*, 680−685.
(29) Bradford, M. M. A rapid and sensitive method for the quantitation of microgram quantities of protein utilizing the principle of protein-dye binding. *Anal. Biochem.* **1976**, *72* (1−2), 248−254.
(30) Bernard-Granger, G.; Guizard, C. Spark plasma sintering of a commercially available granulated zirconia powder: I. Sintering path and hypotheses about the mechanism (s) controlling densification. *Acta Mater.* **2007**, *55* (10), 3493−3504.
(31) Juang, H. Y.; Hon, M. H. Fabrication and mechanical properties of hydroxyapatite-alumina composites. *Mater. Sci. Eng., C* **1994**, *2* (1), 77−81.
(32) Mazaheri, M.; Mari, D.; Schaller, R.; Bonnefont, G.; Fantozzi, G. Processing of yttria stabilized zirconia reinforced with multi-walled carbon nanotubes with attractive mechanical properties. *J. Eur. Ceram. Soc.* **2011**, *31* (14), 2691−2698.
(33) Taheri, M.; Mazaheri, M.; Golestani-Fard, F.; Rezaie, H.; Schaller, R. High/room temperature mechanical properties of 3Y-TZP/CNTs composites. *Ceram. Int.* **2014**, *40* (2), 3347−3352.
(34) Dubey, A. K.; Sitesh, G.; Nath, S.; Basu, B. Spark plasma sintering to restrict sintering reactions and enhance properties of hydroxyapatite−mullite biocomposites. *Ceram. Int.* **2011**, *37* (7), 2755−2761.
(35) Feng, P.; Niu, M.; Gao, C.; Peng, S.; Shuai, C. A novel two-step sintering for nano-hydroxyapatite scaffolds for bone tissue engineering. *Sci. Rep.* **2015**, *4*, 5599.
(36) Zhong, H.; Wang, L.; Fan, Y.; He, L.; Lin, K.; Jiang, W.; Chang, J.; Chen, L. Mechanical properties and bioactivity of β-Ca2 SiO4 ceramics synthesized by spark plasma sintering. *Ceram. Int.* **2011**, *37* (7), 2459−2465.
(37) Li, W.; Gao, L. Fabrication of HAp−ZrO 2 (3Y) nano-composite by SPS. *Biomaterials* **2003**, *24* (6), 937−940.
(38) Afzal, M. A. F.; Kesarwani, P.; Reddy, K. M.; Kalmodia, S.; Basu, B.; Balani, K. Functionally graded hydroxyapatite-alumina-zirconia biocomposite: synergy of toughness and biocompatibility. *Mater. Sci. Eng., C* **2012**, *32* (5), 1164−1173.
(39) Chiba, A.; Kimura, S.; Raghukandan, K.; Morizono, Y. Effect of alumina addition on hydroxyapatite biocomposites fabricated by underwater-shock compaction. *Mater. Sci. Eng., A* **2003**, *350* (1), 179−183.
(40) Aminzare, M.; Eskandari, A.; Baroonian, M.; Berenov, A.; Razavi Hesabi, Z.; Taheri, M.; Sadrnezhaad, S. Hydroxyapatite nanocomposites: Synthesis, sintering and mechanical properties. *Ceram. Int.* **2013**, *39* (3), 2197−2206.
(41) Wang, Y.; Zhang, S.; Zeng, X.; Ma, L. L.; Weng, W.; Yan, W.; Qian, M. Osteoblastic cell response on fluoridated hydroxyapatite coatings. *Acta Biomater.* **2007**, *3* (2), 191−197.
(42) Van'T Hof, R. J.; Ralston, S. H. Nitric oxide and bone. *Immunology* **2001**, *103* (3), 255−261.
(43) Wimalawansa, S. J. Nitric oxide and bone. *Ann. N. Y. Acad. Sci.* **2010**, *1192* (1), 391−403.
(44) Ralston, S. H.; Todd, D.; Helfrich, M.; Benjamin, N.; Grabowski, P. S. Human osteoblast-like cells produce nitric oxide and express inducible nitric oxide synthase. *Endocrinology* **1994**, *135* (1), 330−336.
(45) Karsenty, G. Transcriptional control of skeletogenesis. *Annu. Rev. Genomics Hum. Genet.* **2008**, *9*, 183−196.
(46) Granéli, C.; Thorfve, A.; Ruetschi, U.; Brisby, H.; Thomsen, P.; Lindahl, A.; Karlsson, C. Novel markers of osteogenic and adipogenic differentiation of human bone marrow stromal cells identified using a quantitative proteomics approach. *Stem Cell Res.* **2014**, *12* (1), 153−165.
(47) Stein, G. S.; Lian, J. B.; Van Wijnen, A. J.; Stein, J. L.; Montecino, M.; Javed, A.; Zaidi, S. K.; Young, D. W.; Choi, J.-Y.; Pockwinse, S. M. Runx2 control of organization, assembly and activity of the regulatory machinery for skeletal gene expression. *Oncogene* **2004**, *23* (24), 4315.
(48) Maruyama, Z.; Yoshida, C. A.; Furuichi, T.; Amizuka, N.; Ito, M.; Fukuyama, R.; Miyazaki, T.; Kitaura, H.; Nakamura, K.; Fujita, T.; et al. Runx2 determines bone maturity and turnover rate in postnatal bone

DOI: 10.1021/acsbiomaterials.7b00754
ACS Biomater. Sci. Eng. 2018, 4, 1324−1336

development and is involved in bone loss in estrogen deficiency. *Dev. Dyn.* **2007**, *236* (7), 1876−1890.
(49) Khang, D.; Choi, J.; Im, Y.-M.; Kim, Y.-J.; Jang, J.-H.; Kang, S. S.; Nam, T.-H.; Song, J.; Park, J.-W. Role of subnano-, nano-and submicron-surface features on osteoblast differentiation of bone marrow mesenchymal stem cells. *Biomaterials* **2012**, *33* (26), 5997−6007.
(50) Yang, J.; McNamara, L. E.; Gadegaard, N.; Alakpa, E. V.; Burgess, K. V.; Meek, R. D.; Dalby, M. J. Nanotopographical induction of osteogenesis through adhesion, bone morphogenic protein cosignaling, and regulation of microRNAs. *ACS Nano* **2014**, *8* (10), 9941−9953.
(51) Ji, H.; Marquis, P. Sintering behaviour of hydroxyapatite reinforced with 20 wt% Al 2O3. *J. Mater. Sci.* **1993**, *28* (7), 1941−1945.
(52) Wenzel, R. N. Resistance of solid surfaces to wetting by water. *Ind. Eng. Chem.* **1936**, *28* (8), 988−994.
(53) Cassie, A.; Baxter, S. Wettability of porous surfaces. *Trans. Faraday Soc.* **1944**, *40*, 546−551.
(54) Xu, Q.; Yang, Y.; Wang, X.; Wang, Z.; Jin, W.; Huang, J.; Wang, Y. Atomic layer deposition of alumina on porous polytetrafluoroethylene membranes for enhanced hydrophilicity and separation performances. *J. Membr. Sci.* **2012**, *415*, 435−443.
(55) Leese, H.; Bhurtun, V.; Lee, K. P.; Mattia, D. Wetting behaviour of hydrophilic and hydrophobic nanostructured porous anodic alumina. *Colloids Surf., A* **2013**, *420*, 53−58.
(56) Gittens, R. A.; McLachlan, T.; Olivares-Navarrete, R.; Cai, Y.; Berner, S.; Tannenbaum, R.; Schwartz, Z.; Sandhage, K. H.; Boyan, B. D. The effects of combined micron-/submicron-scale surface roughness and nanoscale features on cell proliferation and differentiation. *Biomaterials* **2011**, *32* (13), 3395−3403.
(57) Lee, W. C.; Lim, C. H. Y.; Shi, H.; Tang, L. A.; Wang, Y.; Lim, C. T.; Loh, K. P. Origin of enhanced stem cell growth and differentiation on graphene and graphene oxide. *ACS Nano* **2011**, *5* (9), 7334−7341.
(58) Ben-Nissan, B.; Choi, A. H.; Macha, I., Advances in Bioglass and Glass Ceramics for Biomedical Applications. In *Biomaterials for Implants and Scaffolds*; Springer: Berlin, 2017; pp 133−161. 10.1007/978-3-662-53574-5_5
(59) Channer, G. A.; Eshraghi, A. A.; Xue-zhong, L. Middle ear implants: historical and futuristic perspective. *J. Otol* **2011**, *6* (2), 10−18.
(60) Jahnke, K.; Plester, D. Bioinert ceramic implants in middle ear surgery. *Ann. Otol., Rhinol., Laryngol.* **1981**, *90* (6), 640−642.

DOI: 10.1021/acsbiomaterials.7b00754
ACS Biomater. Sci. Eng. 2018, 4, 1324−1336